Title

Palmitoylation controls the stability of 190 kDa ankyrin-G in dendritic spines and is regulated by ZDHHC8 and lithium

Authors

Piguel, Nicolas H
Sanders, Shaun S
De Simone, Francesca I
et al.

Publication Date

2023

DOI

10.3389/fnmol.2023.1144066

frontiers | Frontiers in Molecular Neuroscience

TYPE Original Research
PUBLISHED 08 March 2023
DOI 10.3389/fnmol.2023.1144066

OPEN ACCESS

EDITED BY
Laurence Goutebroze,
Institut National de la Santé et de la Recherche Médicale,
France

REVIEWED BY
Paul M. Jenkins,
University of Michigan,
United States
Takashi Hayashi,
National Institute of Advanced Industrial Science and Technology (AIST), Japan

*CORRESPONDENCE
Peter Penzes
✉ p-penzes@northwestern.edu

†These authors have contributed equally to this work

SPECIALTY SECTION
This article was submitted to Molecular Signalling and Pathways, a section of the journal Frontiers in Molecular Neuroscience

RECEIVED 13 January 2023
ACCEPTED 14 February 2023
PUBLISHED 08 March 2023

CITATION
Piguel NH, Sanders SS, De Simone FI, Martin-de-Saavedra MD, McCoig E, Dionisio LE, Smith KR, Thomas GM and Penzes P (2023) Palmitoylation controls the stability of 190 kDa ankyrin-G in dendritic spines and is regulated by ZDHHC8 and lithium.
Front. Mol. Neurosci. 16:1144066.
doi: 10.3389/fnmol.2023.1144066

Palmitoylation controls the stability of 190 kDa ankyrin-G in dendritic spines and is regulated by ZDHHC8 and lithium

Nicolas H. Piguel[1], Shaun S. Sanders[2†], Francesca I. De Simone[2†], Maria D. Martin-de-Saavedra[1,3], Emmarose McCoig[1], Leonardo E. Dionisio[1], Katharine R. Smith[4], Gareth M. Thomas[5] and Peter Penzes[1,6,7]*

[1]Department of Neuroscience, Northwestern University Feinberg School of Medicine, Chicago, IL, United States, [2]Shriners Hospitals Pediatric Research Center, Lewis Katz School of Medicine at Temple University, Philadelphia, PA, United States, [3]Department of Biochemistry and Molecular Biology, School of Pharmacy, Instituto Universitario de Investigación en Neuroquímica, Complutense University of Madrid, Madrid, Spain, [4]Department of Pharmacology, University of Colorado School of Medicine, Aurora, CO, United States, [5]Department of Anatomy and Cell Biology, Shriners Hospitals Pediatric Research Center, Lewis Katz School of Medicine at Temple University, Philadelphia, PA, United States, [6]Department of Psychiatry and Behavioral Sciences, Northwestern University Feinberg School of Medicine, Chicago, IL, United States, [7]Northwestern University Center for Autism and Neurodevelopment, Chicago, IL, United States

Introduction: AnkG, encoded by the *ANK3* gene, is a multifunctional scaffold protein with complex isoform expression: the 480 and 270kDa isoforms have roles at the axon initial segment and node of Ranvier, whereas the 190kDa isoform (AnkG-190) has an emerging role in the dendritic shaft and spine heads. All isoforms of AnkG undergo palmitoylation, a post-translational modification regulating protein attachment to lipid membranes. However, palmitoylation of AnkG-190 has not been investigated in dendritic spines. The *ANK3* gene and altered expression of AnkG proteins are associated with a variety of neuropsychiatric and neurodevelopmental disorders including bipolar disorder and are implicated in the lithium response, a commonly used mood stabilizer for bipolar disorder patients, although the precise mechanisms involved are unknown.

Result: Here, we showed that Cys70 palmitoylation stabilizes the localization of AnkG-190 in spine heads and at dendritic plasma membrane nanodomains. Mutation of Cys70 impairs AnkG-190 function in dendritic spines and alters PSD-95 scaffolding. Interestingly, we find that lithium reduces AnkG-190 palmitoylation thereby increasing its mobility in dendritic spines. Finally, we demonstrate that the palmitoyl acyl transferase ZDHHC8, but not ZDHHC5, increases AnkG-190 stability in spine heads and is inhibited by lithium.

Discussion: Together, our data reveal that palmitoylation is critical for AnkG-190 localization and function and a potential ZDHHC8/AnkG-190 mechanism linking AnkG-190 mobility to the neuronal effects of lithium.

KEYWORDS

ANK3, ankyrin-G, dendrite, dendritic spine, palmitoylation, lithium, ZDHHC8

Introduction

S-palmitoylation, a reversible form of post-translational modification regulating protein attachment to lipid membranes, is a critical process used to stabilize proteins in dendritic spines and dendrites (Salaun et al., 2010) and to localize proteins to different neuronal subcompartments (Tortosa and Hoogenraad, 2018). Important synaptic proteins, including neurotransmitter receptors, scaffold proteins, transporters, adhesion molecules, SNAREs, and other trafficking proteins, are palmitoylated (Kang et al., 2008) and palmitoylation also regulates dendrite and synapse morphology (Shah et al., 2019).

The *ANK3* gene encodes multiple isoforms of ankyrin-G (AnkG), of which the 190, 270, and 480 kDa isoforms are the most prominent in the brain (Zhang and Bennett, 1998). The giant 270 and 480 kDa isoforms have been mostly studied for their function in the axon initial segment (AIS; Leterrier and Dargent, 2014) or nodes of Ravier (Nelson and Jenkins, 2017). The 480 kDa isoform has been shown to prevent gamma-aminobutyric acid (GABA) receptor endocytosis and to have an important role in maintaining GABAergic synapses (Tseng et al., 2015). The 190 kDa isoform of AnkG is less well understood in neurons, but in contrast to larger isoforms, has been found to localize to dendritic spines and can be identified in the human postsynaptic density (PSD) fraction (Focking et al., 2016). Within subsynaptic nanodomains in dendritic spine heads and necks, AnkG-190 plays an important role in dendritic spine maintenance and long-term potentiation (Smith et al., 2014).

The membrane-binding regions of all three main AnkG isoforms harbor a cysteine residue (C70) that can be palmitoylated, a process that is required for AnkG association with the membrane, appropriate cellular localization, and function in non-neuronal cells (Thomas et al., 2012; He et al., 2014). Structural analysis has shown that the membrane anchoring of AnkG is facilitated by palmitoylation, defining a stable binding interface on the lipid membrane (Fujiwara et al., 2016). Palmitoylation is known to play an important role in the function of 270 and 480 kDa isoforms, but the role of palmitoylation of the 190 kDa isoform in neurons is unknown (Thomas et al., 2012; Tseng et al., 2015).

The human *ANK3* gene has been associated with various neuropsychiatric diseases, including bipolar disorder (BD), schizophrenia, and autism spectrum disorder (ASD; Schulze et al., 2009; Bi et al., 2012; Yuan et al., 2012). Multiple independent genome-wide association studies (GWAS) have strongly linked *ANK3* to BD in a variety of different ethnicities (Scott et al., 2009; Smith et al., 2009; Tesli et al., 2011; Muhleisen et al., 2014) and have been corroborated by meta-analyses (Roby, 2017). In addition to a genetic association with *ANK3*, some studies have shown an increase in *ANK3* expression in the blood (Wirgenes et al., 2014) and lymphoblastoid cells of BD patients (Kato et al., 2011), revealing the potential involvement of AnkG in disease mechanisms. Furthermore, a BD-related risk variant in *ANK3* is associated with decreased expression of a specific AnkG isoform in the cerebellum (Rueckert et al., 2013), and variants linked to loss of function are also implicated in ASD and intellectual disability (ID; Iqbal et al., 2013). Thus, either an increase or a decrease in *ANK3* gene expression and isoform-specific variation may be implicated in the disorders. Lithium is a mood stabilizer commonly used to treat BD patients as a first-line intervention (Malhi et al., 2017). Responsiveness of BD patients to lithium treatment appears to be a heritable trait (Grof et al., 2002) linked to genetic markers in patients isolated from GWAS (Hou et al., 2016). Interestingly, lithium has been used to correct BD-related behaviors and neuronal architecture deficits in Ank3 expression-deficient mouse models, suggesting a potential link between *ANK3* and the lithium response (Leussis et al., 2013; Gottschalk et al., 2017; Zhu et al., 2017; Piguel et al., 2022).

Understanding synaptic palmitoylation is likely to provide insights into normal neuronal functions and also pathophysiological and therapeutic mechanisms (Thomas et al., 2013). Thus, we investigated the physiological function of AnkG palmitoylation and how it may be regulated by palmitoyl acyl transferases and a mood stabilizer.

Materials and methods

Plasmids and antibodies

AnkyrinG-190-GFP was a gift from Vann Bennett (Addgene plasmid # 31059; http://n2t.net/addgene:31059; RRID: Addgene_31,059). AnkG-mCherry was a gift from Benedicte Dargent (Addgeneplasmid #42566; http://n2t.net/addgene:42566; RRID: Addgene_42,566). HA-ZDHHC5 and HA-ZDHHC8 were kind gifts from Dr. Shernaz Bamji. pEGFP-N2 and pmCherry-C1 (Clontech, Mountain View, CA, United States; now Takara Bio United States, Inc.). The following primary monoclonal and polyclonal antibodies (mAb and pAb, respectively) were used: AnkG mAb clone N106/20 (western blot) and clone N106/36 (immunocytochemistry) from Neuromab (Davis, CA, United States), PSD-95 (Neuromab), turboGFP mAb (to identify RNAi expression, Origene, United States), DsRed pAb (to identify mCherry expression, Clontech, Mountain View, CA, United States), and GFP chicken pAb (to identify GFP expression, Abcam, Cambridge, MA, United States).

Neuronal cell culture and transfection

Dissociated cultures of primary cortical neurons were prepared from E18 Sprague–Dawley rat embryos. Brains were dissected in ice-cold Hank's buffered salt solution, and cortical tissue was isolated, digested with papain (Sigma; diluted in Neurobasal with EDTA (0.5 mM) and DNaseI (2 units/ml), activated with L-cysteine (1 mM) at 37°C), and mechanically dissociated in neuronal feeding media (Neurobasal + B27 supplement (Invitrogen, Carlsbad, CA, United States) + 0.5 mM glutamine + penicillin/streptomycin). Dissociated neurons were plated at high density (300,000 cells/cm^2) on 1.5 mm thickness polylysine-coated glass coverslips of 18 mm diameter (Warner Instrument, Hamden, CT, United States). One hour after plating, the media was replaced. Neuronal cultures were maintained at 37°C in 5% CO_2. The neuronal feeding medium was supplemented with 200 μM D,L-amino-phosphonovalerate (D,L-APV, Ascent Scientific, Bristol, United Kingdom) beginning on day 4 *in vitro* (DIV4). Neurons were transfected at DIV21 with Lipofectamine 2000 (Invitrogen), providing a transfection efficiency of 0.5%–1%. Plasmids (2–5 μg total DNA). Briefly, Lipofectamine 2000 and DNA were diluted in Dulbecco's Modified Eagle Medium + HEPES (10 mM), mixed thoroughly together, and incubated for 20–30 min at 37°C before addition to cultured cells in the absence of antibiotics. Following transfection, neurons were supplanted in

antibiotic-containing feeding media containing half conditioned and half fresh media and allowed to express constructs for 3 days or as indicated.

Immunocytochemistry

Cells were fixed for 10 min in 4% formaldehyde/4% sucrose in PBS and then in methanol pre-chilled to −20°C for 10 min. Fixed neurons were permeabilized and blocked simultaneously in PBS containing 2% normal goat serum and 0.2% Triton-X-100 for 1 h at room temperature. Primary antibodies were added in PBS containing 2% normal goat serum overnight at 4°C, followed by 3 × 10 min washes in PBS. Secondary antibodies were incubated for 1 h at room temp, also in 2% normal goat serum in PBS. Three further washes (15 min each) were performed before coverslips were mounted using ProLong antifade reagent (Life Technologies).

Confocal microscopy

Confocal images of immunostained neurons were obtained with a Nikon (Amsterdam, Netherlands) C2 confocal microscope. Images of neurons were taken using the 63x oil-immersion objective [numerical aperture (NA) = 1.4] as z-series of 7–12 images taken at 0.4 µm intervals, averaged 2 times, with 1,024 × 1,024 pixel resolution. Detector gain and offset were adjusted in the channel of each cell fill (GFP or mCherry) to include all spines and enhance edge detection. Intensity plot profiles for dendrite/spine localization were performed in ImageJ. A 4 µm line was drawn across 3–5 spines per neuron and averaged across neurons to produce average intensity plot profiles ± SEM. Spine density, width, and length were analyzed with ImageJ. Epifluorescence images were obtained with a 10x objective, and traces of dendrites were drawn and analyzed with Sholl analysis in ImageJ. In culture, pyramidal neurons conserve their polarity and develop a long dendrite, which we refer to as the apical dendrite, and shorter dendrites near the soma, which we refer to as basal dendrites for Sholl analysis.

Structured illumination microscopy imaging and analysis

Imaging and reconstruction parameters were empirically determined with the assistance of the expertise in the Nikon Imaging Center at Northwestern. The acquisition was set to 10 MHz, 14 bits with EM gain, and no binning. Auto-exposure was kept between 100 and 300 ms, and the EM gain multiplier was restrained below 300. Conversion gain was held at 1x unless necessary to increase the signal to 2.4×. Laser power was adjusted to keep max pixel intensity < 4,000 units. Three reconstruction parameters (illumination modulation contrast, high-resolution noise suppression, and out-of-focus blur suppression) were extensively tested to generate consistent images across experiments without abnormal features or artifacts and produce the best Fourier transforms. Reconstruction parameters (0.96, 1.19, and 0.17) were kept consistent across experiments and imaging sessions. 3D dendritic spine reconstruction was done on a NIS instrument (Nikon). Intensity plot profiling for dendrite analysis was performed with ImageJ (National Institutes of Health, http://rsbweb.nih.gov/ij). A punctate distribution at the membrane corresponds to a larger fluctuation in fluorescence intensity, which will result in a larger standard deviation (Puncta index).

Pharmacological treatments

2-Bromopalmitate (2-BrP), a palmitoylation inhibitor, and S-methyl methanethiosulfonate (MMTS), a thiol blocker, were from Sigma (St. Louis, MO, United States). All other chemicals were from ThermoFisher Scientific (Waltham, MA, United States) and were of the highest reagent grade. 2-BrP was used at 20 mM, palmostatin B (which inhibits depalmitoylation) at 50 µM, lithium chloride at 2 mM, and all were applied for stimulation over 24 h.

Acyl biotinyl exchange assay

For acyl biotinyl exchange (ABE) experiments, rat cortical neurons cultured as described above were lysed directly in buffer (50 mM HEPES pH 7.0, 2% SDS, 1 mM EDTA) plus protease inhibitor mixture (PIC, Roche) and 20 mM MMTS (to block free thiols). Following lysis, excess MMTS was removed by acetone precipitation. Pellets were dissolved in a buffer containing 4% (wt/vol) SDS. Samples were diluted and incubated for 1 h in either 0.7 M hydroxylamine (NH_2OH) pH 7.4 (to cleave thioester bonds) or 50 mM Tris pH 7.4, both containing sulfhydryl-reactive (HPDP-) biotin and incubated for 1 h at room temperature. Acetone precipitation was performed to remove unreacted HPDP-biotin and hydroxylamine and pellets were resuspended in lysis buffer without MMTS. SDS was diluted to 0.1% (wt/vol) and biotinylated proteins in the samples were affinity-purified using neutravidin-conjugated beads. Beta-mercaptoethanol [1% (vol/vol)] was used to cleave HPDP-biotin and release purified proteins from the beads. The released proteins in the supernatant were denatured in the SDS sample buffer and processed for SDS-PAGE. Adult rat forebrain was dissected, rapidly cooled in ice-cold recording buffer (Thomas et al., 2012), and homogenized in 10 volumes of 4 mM HEPES, 320 mM sucrose, pH 7.4, containing fresh PIC and 20 mM MMTS. Samples were centrifuged to remove debris, brought to room temperature, and SDS was added to 1% (v/v) final concentration. Samples were then centrifuged at 27,000 ×*g* for 30 min at 4°C and supernatants were subjected to acetone precipitation and ABE as described above.

Fluorescence recovery after photobleaching

Neurons were imaged at 37°C, 5% CO_2, with a Nikon C2 confocal microscope using a 63x oil immersion objective with NA = 1.4 in an OKOLAB stage-type CO_2 incubator. Single plane images were captured with an EMCCD camera every 10 s for 200 s. 80% laser power pulses of 1 ms (2 iterations) were used to bleach GFP in the spine. After background subtraction and validation of the maximum 10% remaining fluorescence after photobleaching, data were normalized with the pre-bleach value. Recovery data points were then fitted to a one-phase association exponential in GraphPad Prism. The

10.3389/fnmol.2023.1144066

mobile fraction was calculated as an average of the plateaued fluorescence level and expressed as a percentage of the pre-bleached level.

Statistical analysis

All statistical tests were performed with GraphPad Prism. Data were tested for normality with D'Agostino and Pearson methods to determine the use of non-parametric (Mann–Whitney, Kruskal–Wallis, Spearman correlations) or parametric (unpaired *t*-test, ANOVA, Pearson correlations) tests. *Post-hoc* tests were included in analyses with multiple comparisons. Bar graphs the mean ± SEM unless otherwise noted. Differences were considered significant if $p < 0.05$. *N* values refer to the number of cells per condition from a minimum of three biological replicates unless otherwise stated.

Results

Palmitoylation of C70 stabilizes AnkG-190 in dendritic spine heads and dendritic nanodomains

We have previously demonstrated that AnkG-190 plays a key role in the dendritic spine and dendrite maintenance (Smith et al., 2014). However, the post-translational modifications that regulate these specific functions of AnkG-190 are unknown. Since palmitoylation of AnkG-190 in non-neuronal cells was shown to be essential for the association of AnkG with plasma membranes (Thomas et al., 2012; He et al., 2014; Fujiwara et al., 2016), we hypothesized that this modification may also modulate AnkG-190's localization in dendrites. We first validated the presence of palmitoylated AnkG-190 in rat cortex utilizing the acyl-biotinyl exchange assay (Thomas et al., 2012), which exchanges palmitoyl modifications to biotin (Figure 1A). To prevent palmitoylation of AnkG-190, we mutated the cysteine 70 residue (Thomas et al., 2012) to alanine (C70A) in a GFP fused construct (GFP-AnkG-190-C70A) and assessed how palmitoylation-deficient AnkG-190 could localize in neuronal dendrites and dendritic spines (Figure 1B). Confocal images revealed that overexpressed GFP-AnkG-190-WT is enriched in the spine head, as previously observed (Smith et al., 2014). This enrichment is lost after the cysteine 70 residue is mutated to alanine (Figure 1C). Quantification revealed abrogation of GFP-AnkG-190-C70A spine head localization comparable to soluble GFP cell fill level (Figure 1D). To assess localization of AnkG-190-C70A in dendritic spines, we used super-resolution structured illumination microscopy (SIM) imaging (Smith et al., 2014; Crosby et al., 2019). Dendritic spine SIM imaging confirmed the results obtained by confocal microscopy. However, AnkG-190-C70A prevented the formation of these nanodomains present in the spine head observed when the AnkG-190-WT construct was expressed (Figure 1E). SIM imaging of dendrites showed that the C70A point mutation did not alter the presence of AnkG-190 at the membrane but changed its localization pattern (Figure 1F). AnkG-190-C70A was found to exhibit a more diffuse distribution pattern compared to AnkG-190-WT (Figures 1F,G) measured by a smaller variation in fluorescence intensity (Puncta index). These results indicate that palmitoylation is important to maintain nanodomains within dendritic spines and along the dendrite.

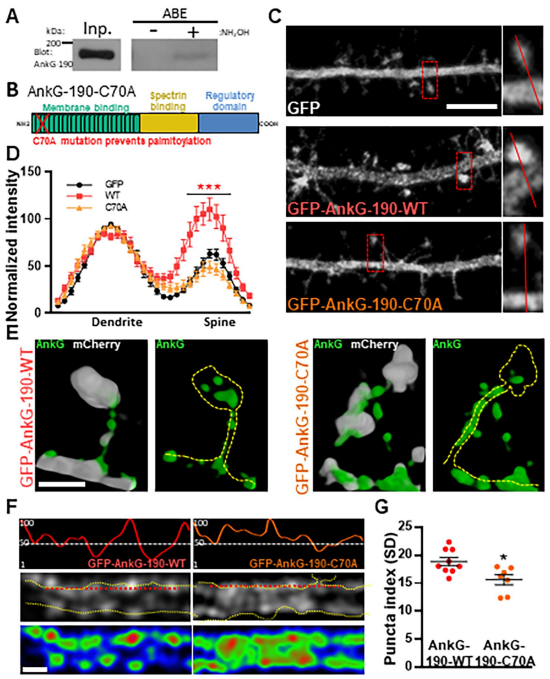

FIGURE 1
Palmitoylation of cysteine 70 stabilizes AnkG-190 in dendritic spines and dendrites. **(A)** AnkG-190 is palmitoylated in rat forebrain. Solubilized rat forebrain homogenates were subjected to ABE to purify palmitoylated proteins. ABE fractions and a portion of input homogenate (Inp.) were western blotted to detect AnkG. Exclusion of NH_2OH was used as a control for assay specificity. **(B)** Schematic of 190kDa Ankyrin-G isoform showing the mutated cysteine which prevents palmitoylation. **(C)** Confocal images of 24-day cultured cortical neurons expressing mCherry with GFP, GFP-AnkG-190-WT, or GFP-AnkG-190-C70A for 1day, scale=5µm. **(D)** Linescan analysis of spine:dendrite ratio of expressed GFP, GFP-AnkG-190-WT, or GFP-AnkG-190-C70A (16–20 neurons per condition, 2-way ANOVA with Dunnett's post-test, ***$p < 0.001$, ±SEM). **(E)** Spine SIM imaging 3D reconstruction of cultured rat neurons expressing mCherry (white), GFP-AnkG-190-WT, or GFP-AnkG-190-C70A (both green), scale=0.5µm. **(F)** SIM imaging of dendrites from cultured cortical neurons expressing GFP-AnkG-190 or GFP-AnkG-190-C70A, scale=0.5µm, in gray or pseudocolor (middle and bottom) and their associated normalized linescan (top). **(G)** Scatter plot of the puncta index average (7–9 neurons per condition, Mann Whitney, *$p < 0.05$, ±SEM) for GFP-AnkG-190-WT or GFP-AnkG-190-C70A overexpression.

AnkG-190-C70A overexpression modifies dendritic spines density and PSD95 spine content

After establishing that the C70A mutation altered AnkG localization, we analyzed the impact of the palmitoylation-deficient AnkG-190 on dendritic spine morphology and PSD-95 content, two parameters modified by the increase of AnkG-190 (Smith et al., 2014). We tested this by quantitative analysis of spine linear density and morphology in neurons coexpressing mCherry with wild-type or GFP-AnkG-190-C70A (Figure 2A). Compared to GFP-AnkG-190-WT, the mutated form had fewer dendritic spines which were

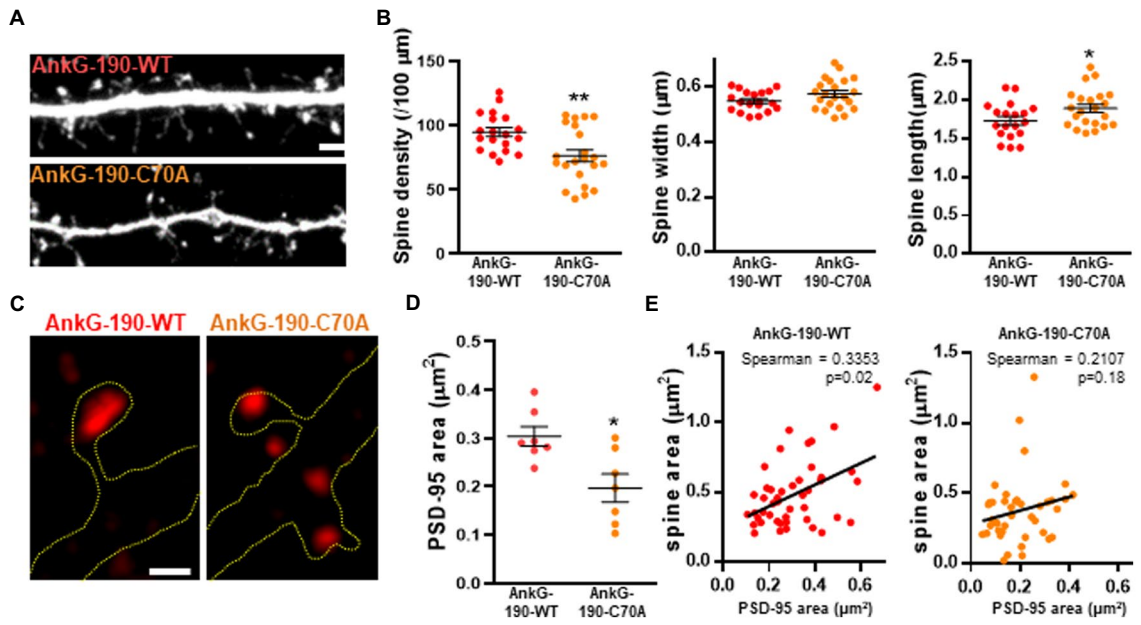

FIGURE 2
Effect of AnkG-190-C70A overexpression on dendritic spines. **(A)** Confocal images cultured cortical neurons expressing mCherry with GFP-AnkG190-WT or GFP-AnkG190-C70A, scale=5µm. **(B)** Scatter plots showing quantification of spine density, spine width, and spine length for neurons expressing mCherry with GFP-Ank-G190-WT or GFP-AnkG-190-C70A (n =19–22 neurons, 1-way ANOVA with a Dunnett's post-test, *$p < 0.005$, **$p < 0.01$, ±SEM). **(C)** SIM images of PSD-95 from GFP-AnkG-190-WT and GFP-AnkG-190C-70A expressing, scale=0.5µm. **(D)** Scatter plot graph showing a decrease of PSD-95 area in the spine with C70A mutation compared with WT (n =7 neurons, Mann Whitney, *$p < 0.05$, ±SEM). **(E)** Correlation plot of spine area vs. PSD-95 area (40 to 50 spines) for GFP-AnkG-190-WT or GFP-AnkG-190-C70A overexpression.

associated with a longer neck (Figure 2B). The mutation did not cause any differences to spine width. AnkG-190 has been previously shown to increase the dendritic spine head (Smith et al., 2014) and we would expect an increase in synaptic scaffold proteins (Meyer et al., 2014). Therefore, we decided to analyze PSD-95, a key component of post-synaptic density. Surprisingly, the C70A mutation showed a smaller PSD-95 area in spine heads as compared to GFP-AnkG-190-WT (Figures 2C,D). To assess whether the reduction of PSD-95 was associated with a change in spine size, we compare the size of PSD-95 puncta in the spine head with the area of the corresponding spine head. We observed a significant positive correlation between spine size and PSD-95 content (Figure 2E). Interestingly, this positive correlation was lost when neurons were transfected with AnkG-190-C70A suggesting the importance of palmitoylation for the AnkG-190 to maintain PSD-95 in the spine. Taken together, these data show that AnkG-190 palmitoylation is important to maintain dendritic spine density and PSD-95 in the spine head.

Lithium reduces AnkG-190 palmitoylation and increases its mobility

To investigate lithium-dependent modifications of AnkG, we performed an acyl biotinyl exchange (ABE) assay in cortical neuron cultures followed by western blotting of AnkG. We used an acute treatment of 2 mM of lithium chloride, a concentration able to phosphorylate 50% of GSK3β (Klein and Melton, 1996; Rao et al., 2005), over 24 h. Interestingly, treatment with lithium resulted in a ~58% decrease in palmitoylated AnkG-190 (Figures 3A,B), a level similar to the negative condition containing the palmitoylation inhibitor 2-Bromopalmitate. On the other hand, lithium was not able to reduce GRIP1 palmitoylation (Figures 3C,D), another protein present in dendritic spines, demonstrating a level of specificity for AnkG-190. Consistent with a reduction in palmitoylation, immunocytochemistry of cortical neuron cultures after lithium treatment revealed a decrease in endogenous AnkG staining in mature spines (width ≥ 0.8 µm), which contain higher levels of AnkG (Smith et al., 2014), compared to vehicle treatment (Figures 3E,F). These data demonstrate that lithium reduces the amount of AnkG localized in spines, which is consistent with the localization of palmitoylation-deficient AnkG. This result led us to hypothesize that lithium could prevent palmitoylation of AnkG-190 and therefore increase AnkG mobility in spines. To test this hypothesis, we performed fluorescence recovery after photobleaching (FRAP) in neurons overexpressing AnkG-190 and treated them with lithium for 24 h (Figures 3G–I). Interestingly, lithium treatment increased the mobile fraction of GFP-AnkG-190-WT from ~52% to ~75% (Figure 3G) comparable to the GFP-AnkG-190-C70A which cannot be palmitoylated. Moreover, lithium treatment did not affect the AnkG-190-C70A mobility suggesting the need for the palmitoylation site for the lithium action. These data support the effect of lithium on the reduction of AnkG-190 palmitoylation leading to an increase in its mobility.

Lithium prevents ZDHHC8 to stabilize AnkG-190 in dendritic spines

Specificity in palmitoylation is achieved through the activity of various related palmitoyl acyl transferases (PATs) proteins. Lithium was found to decrease the palmitoylation of AnG-190, but not that of GRIP1,

10.3389/fnmol.2023.1144066

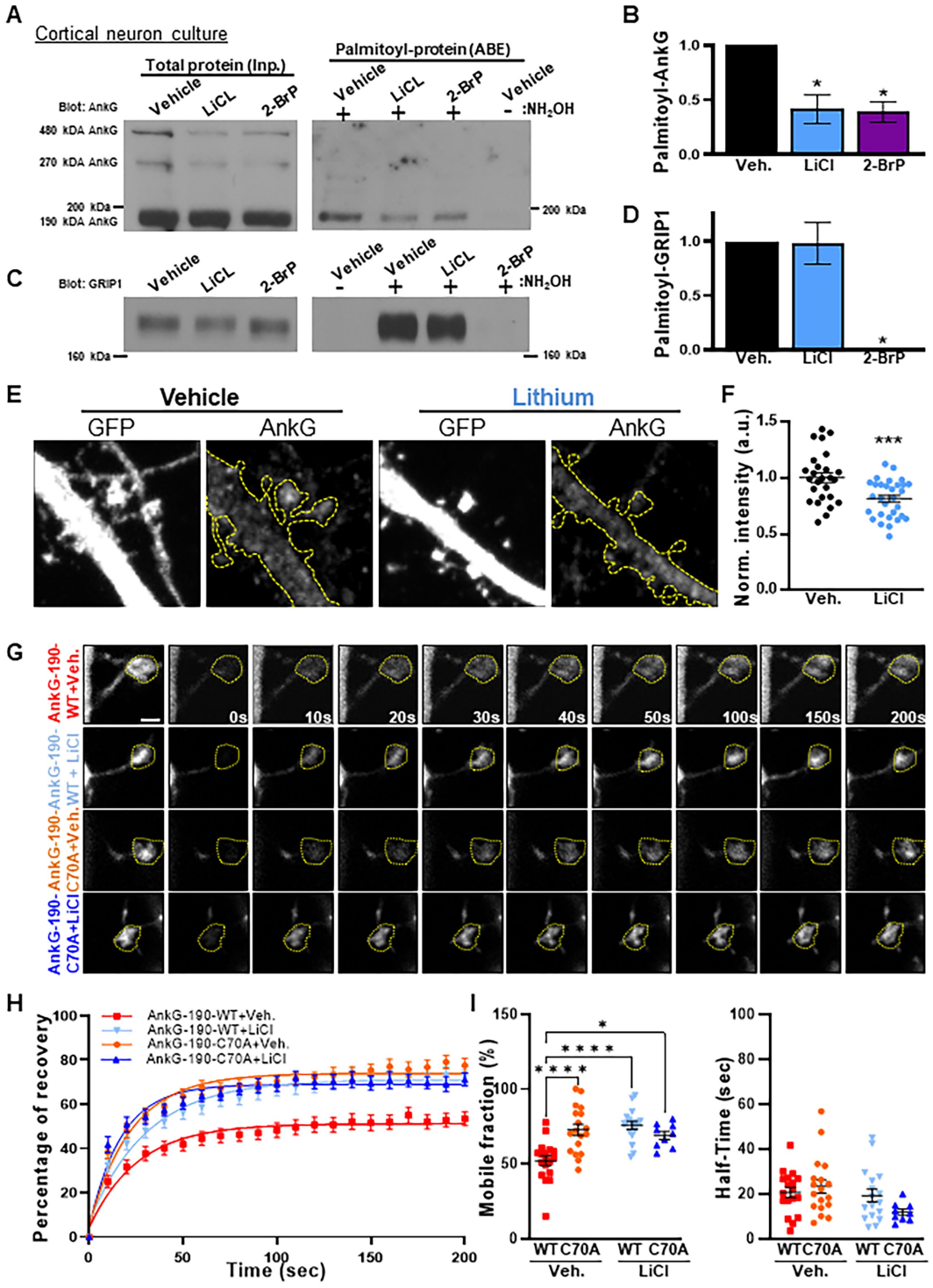

FIGURE 3
Lithium induces a decrease of palmitoylated AnkG-190 isoform and increases its mobility. **(A)** Lysates of cortical neurons treated with the indicated compounds were subjected to ABE to purify palmitoylated proteins. Levels of palmitoyl-AnkG-190 (right blot) and total AnkG expression in parent lysates (left blot bottom blot) were detected with specific antibodies. Exclusion of NH_2OH was used as a control for assay specificity. **(B)** Bar graph of 190kDa AnkG isoform palmitoylation normalized with the input and relative to the untreated condition (5 independent experiments, *t*-test, $*p < 0.05$, ±SEM). **(C)** Lysates of cortical neurons treated with the indicated compounds were subjected to ABE to purify palmitoylated proteins. Levels of palmitoyl-GRIP1 (right blot) and total AnkG expression in parent lysates (left blot) were detected with specific antibodies. Exclusion of NH_2OH was used as a control for assay specificity. **(D)** Bar graph of GRIP1 palmitoylation normalized with the input and relative to the untreated condition (4 independent experiments, Kruskal–Wallis with Dunn's post-test, $*p < 0.05$, ±SEM). **(E)** Representative maximal projection of a confocal image of endogenous AnkG staining in cortical neurons transfected with GFP with or without lithium stimulation, scale=2µm. **(F)** Scatter plot of AnkG average intensity in mushroom spines on a single plane (26–30 neurons on 3 independent experiments, *t*-test, $***p < 0.001$, ±SEM). **(G)** Representative time-lapse images of GFP-AnkG-190 fluorescence in 24 days rat neurons culture overexpressing GFP-AnkG-190-WT or GFP-AnkG-190-C70A for 3days +/− lithium chloride during 1day in FRAP experiments, scale=2µm. **(H)** Quantification of GFP fluorescence in spines over time. Data are fitted with single exponentials (colored lines). Data are represented as mean±SEM. **(I)** Scatter plots of mobile fraction (left) or half-time recovery (right) of GFP-AnkG-190-WT or GFP-AnkG-190-C70A +/− lithium chloride (n =9–18 neurons, two-way ANOVA with Tukey post-test, $****p \leq 0.0001$, $*p < 0.05$, ±SEM).

10.3389/fnmol.2023.1144066

within neurons, suggesting a targeted effect of lithium on a subset of neuronal palmitoylated proteins. PATs that have the capability of palmitoylating AnkG have been described in HEK293 and MDCK cells and include ZDHHC5 and ZDHHC8. These PATs target the C70 residue on AnkG-190, but it is unknown whether a similar mechanism occurs in neurons (He et al., 2014). By using overexpression and FRAP imaging in neuron cultures, we assessed whether ZDHHC5 and/or ZDHHC8 were able to stabilize AnkG-190 in dendritic spines and if lithium could reverse the process. To ensure the spine mobility phenotypes were palmitoylation-dependent, we also treated cultures with Palmostatin B, an inhibitor of thioesterase APT1 and APT2 (Rusch et al., 2011), which effectively block the depalmitoylation pathway. We found that ZDHHC5 did not affect the recovery of fluorescence of GFP-AnkG-190 (Figures 4A–C) demonstrating that it does not modulate AnkG-190 mobility in spines. In contrast, ZDHHC8 significantly decreased the GFP-AnkG-190 mobile fraction in the dendritic spine (Figures 4A,D,E), suggesting it can palmitoylate AnkG-190 and stabilize the protein in the dendritic spine. Moreover, we found that lithium treatment can inhibit the effects of ZDHHC8 overexpression on GFP-AnkG-190 confirming its action on the palmitoylation process.

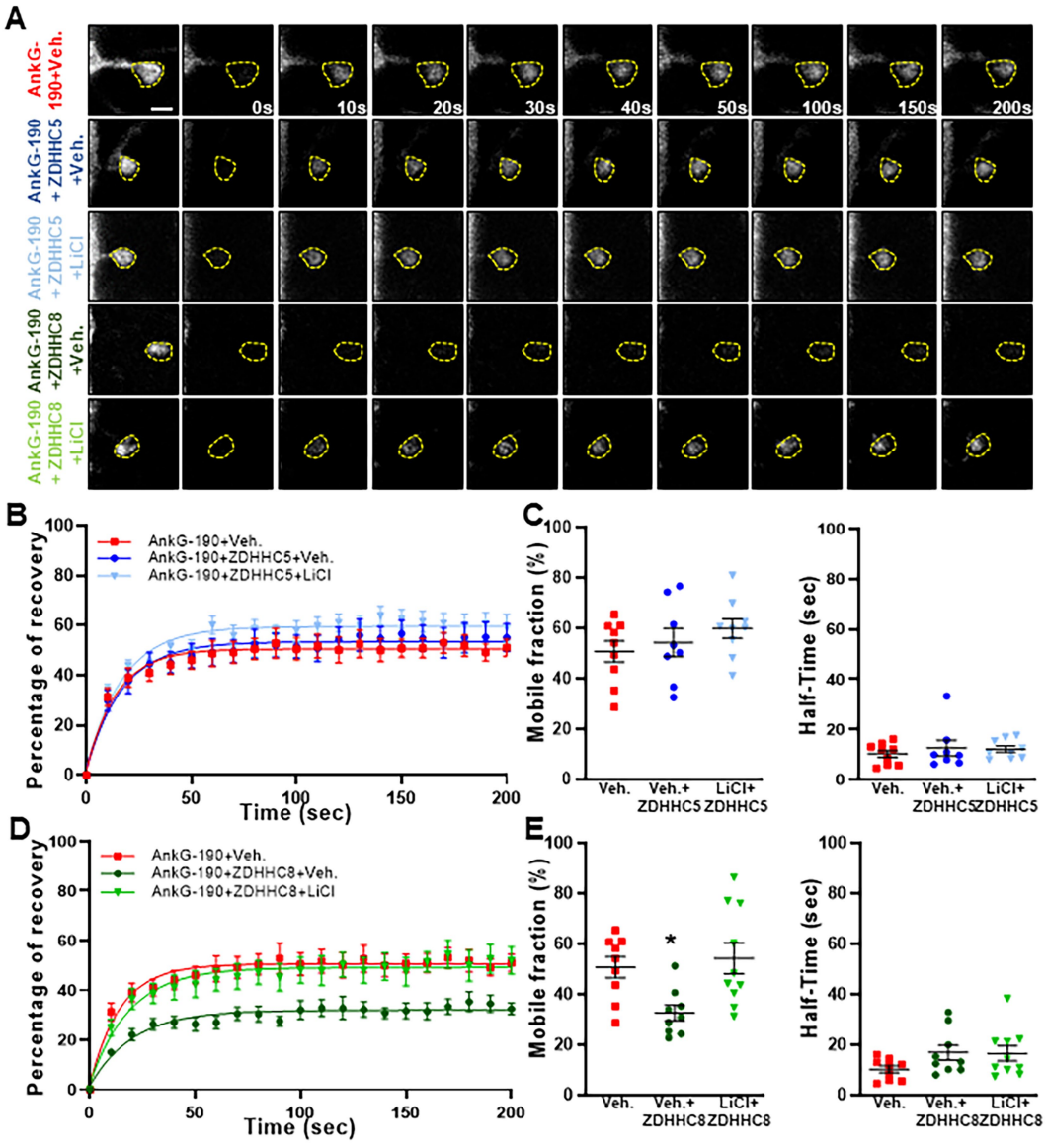

FIGURE 4
Lithium prevents ZDHHC8 to stabilize AnkG-190 in dendritic spines. **(A)** Representative time-lapse images of GFP-AnkG-190 fluorescence in 24days rat neurons culture overexpressing GFP-AnkG-190 with or without ZDHHC5 or ZDHHC8 during 3days in FRAP experiments, scale=2μm. Cultures are treated with palmostatin B +/− lithium chloride 24h prior to the experiment. **(B)** Quantification of GFP fluorescence in spines over time. Data are fitted with single exponentials (colored lines). Data are represented as mean±SEM. **(C)** Scatter plots of mobile fraction (left) or half-time recovery (right) of GFP-AnkG-190 in the presence or absence of ZDHHC5 +/− lithium chloride (n =8–10 neurons, one-way ANOVA with Dunnett's post-test). **(D)** Quantification of GFP fluorescence in spines over time. Data are fitted with single exponentials (colored lines). Data are represented as mean±SEM. **(E)** Scatter plots of mobile fraction (left) or half-time recovery (right) of GFP-AnkG-190 in the presence or absence of ZDHHC8 +/− lithium chloride (n =8–10 neurons, one-way ANOVA with Dunnett's post-test, *$p < 0.05$, ±SEM) **B** and **D** share the same control and only one-way ANOVA was performed for the mobile fraction and the half-time including the 5 conditions and separated between **C** and **E** for better clarity.

Discussion

In the present study, we showed that palmitoylation of cysteine 70 stabilizes the localization of AnkG-190 in spine heads and at dendritic plasma membrane nanodomains. Remarkably, overexpression of a mutant AnkG-190 lacking this palmitoylation presents less PSD-95 in dendritic spine heads compared to the wild-type protein. We demonstrated that lithium treatment reduced AnkG-190 palmitoylation and increased its mobility in spines in a ZDHHC8-dependent pathway. Taken together, our data revealed a role for palmitoylation in dendritic spine components and uncovered a novel mechanism of lithium action on AnkG-190.

AnkG-190 shares most of it is protein domains with the longer AnkG-480 isoform and we would expect it to play a similar role in neurons. However, previous studies described a dendritic location of the AnkG-190 which can especially be found in dendritic spines (Smith et al., 2014) and PSD fractions (Focking et al., 2016). Unlike the longer isoforms specific to the brain, AnkG-190 is expressed in other organs and has been studied in epithelial cells, where it plays a role in lateral membranes (Kizhatil et al., 2007a; Jenkins et al., 2013) and where it is associated with βII-Spectrin (Kizhatil et al., 2007b; Jenkins et al., 2015a). As in epithelial cells or for the neuronal AnkG-270 isoform (He et al., 2012), we showed that cysteine 70 is important for AnkG-190 localization in neuron dendrites. The C70A mutated AnkG-190 protein failed to form nanodomains in dendrites and dendrite spine heads. Our group showed previously that those nanodomains surround the PSD-95 area present in the dendritic spine and their increased number is significantly correlated to a bigger PSD95 area. Moreover, overexpression of AnkG-190 significantly increased the size of the spine head (Smith et al., 2014). Unlike AnkG-190-WT, AnkG-190-C70A does not lead to an increase of PSD-95 area but still affects the spine width suggesting AnkG-190 nanodomains stabilize PSD-95 but not the spine head architecture. Dendritic spine volume and PSD-95 size are linearly related (Cane et al., 2014) but the loss of PSD-95 is not a prerequisite for spine retraction (Woods et al., 2011) and AnkG-190 could serve as a link between the PSD and the cytoskeleton to maintain the correlation between the dendritic spine and PSD-95 volume. Although spine width does not significantly change, we can see a reduction in dendritic spine density and dendritic spine length, possibly due to a change of location AnkG-190 which will modify the localization of other proteins including dendritic spine initiators. We previously described a role for AnkG-190 in dendritic spine necks (Smith et al., 2014) and the absence of palmitoylation could redistribute AnkG-190 to the spine neck, consequently affecting the spine length.

AnkG-190 localization is not lost at the membrane or in the dendritic spine neck suggesting AnkG-190 can be stabilized by other protein interaction partners like spectrin (Smith et al., 2014). Unpalmitoylated AnkG has higher mobility within spines, indicating that palmitoylation restricts its mobility to specific sites, but still conserves a smaller stable population. These data suggest that only a subset of AnkG is palmitoylated at Cysteine 70 and other subpopulations of AnkG-190 exist in spines with distinct roles. Another possible protein interaction that can maintain AnkG-190 in the dendritic spine is the scaffold protein Homer1, which can bind Shank proteins to regulate spine morphology (Hayashi et al., 2009). Homer1 can bind directly to the PPXXF motif within AnkG-190 through it is EVH1 domain. Interestingly, mutation of the PPXXF motif induces a loss of AnkG-190 localization, which does not affect all of the immobile fraction, similar to AnkG-190-C70A (Yoon et al., 2021).

Lithium has been shown to rescue some BD-related behavioral deficits in different *Ank3* KO mouse models (Leussis et al., 2013; Gottschalk et al., 2017; Zhu et al., 2017), suggesting it can alleviate symptoms of mouse models with AnkG loss of function. However, heterozygous and homozygous loss of *ANK3* likely represent rare mutations only present in a small subset of patients with ASD and ID, and the majority of individuals with BD are likely to retain AnkG expression or have increased expression (Kato et al., 2011; Wirgenes et al., 2014; Hughes et al., 2018). Moreover, the deletion of exon 37, present in 270 and 480 kDa isoforms, induces a fivefold expression increase of the AnkG-190 isoform (Jenkins et al., 2015b). Therefore AnkG-dependent mechanisms may also play a role in the lithium response. We showed in neuron culture that lithium treatment has a drastic effect on AnkG-190 palmitoylation reducing it at the same level as the 2-BrP condition, suggesting lithium blocks the entire pool of unpalmitoylated AnkG-190 to be palmitoylated. Furthermore, the reduction of endogenous AnkG in the spine head and increase of the GFP-AnkG-190 mobile fraction in the dendritic spine supports the reduction of palmitoylation observed. In our previous work, acute lithium stimulation was not able to change dendritic spine density and even increased spine head width (Piguel et al., 2022) whereas chronic treatment has been shown to reduce dendritic spine density without affecting mushroom spine head diameter (Khayachi et al., 2021). Moreover, this study shows a reduction of PSD95 expression including a decrease in PSD95 puncta intensity. Those phenotypes seem to recapitulate the difference between AnkG-190-WT and AnkG-190-C70A overexpression suggesting the reduction of AnkG-190 palmitoylation could be an early event to the drastic change observed during the chronic lithium treatment.

Only ZDHHC8, one of the two PATs described to palmitoylate AnkG-190 (Thomas et al., 2012), can stabilize GFP-AnkG-190 in the dendritic spine when it was overexpressed. This effect was abolished after 24 h of lithium stimulation supporting the decrease of AnkG-190 palmitoylation due to the inhibition of ZDHHC8 activity. Moreover, palmitoylated GRIP1, which is also a target of ZDDHC8 too (Thomas et al., 2012), is not decreased during lithium treatment indicating a specific inhibition of AnkG-190 palmitoylation. Although ZDHHC5 and ZDDHC8 seem to share some of their targets such as AnkG, GRIP1, or PICK1, the two PATs do not present the same staining pattern in neurons (Thomas et al., 2012). Therefore, we cannot exclude that ZDHHC5 alters the stability of AnkG-190 outside of dendritic spines, as ZDHHC proteins are known to have specific effects in neuronal sub-compartments (Thomas et al., 2013). While *ZDHHC8* has not been yet associated with BD (Otani et al., 2005), it has been related to schizophrenia (Qin et al., 2020) and epilepsy (Yang et al., 2018) overlapping with *ANK3* (Lopez et al., 2017).

Our work describes a new mechanism of mood stabilizer action and its effects on two important psychiatric disorder risk factors *ANK3* and *ZDHHC8*. These findings open new directions for understanding basic control of neuroarchitecture but may also provide new opportunities for novel therapeutic targets.

Data availability statement

The raw data supporting the conclusions of this article will be made available by the authors, without undue reservation.

Ethics statement

The animal study was reviewed and approved by Institutional Animal Care and Use Committee at Northwestern University.

Author contributions

NP, GT, and PP designed research. NP, FD, SS, MM, EM, LD, and KS performed research. NP, FD, and SS analyzed data. NP and PP wrote the paper. All authors contributed to the article and approved the submitted version.

Funding

This work was supported by R01MH107182 to PP Imaging work was performed at the Northwestern University Center for Advanced Microscopy, generously supported by NCI CCSG P30 CA060553 awarded to the Robert H. Lurie Comprehensive Cancer Center.

Acknowledgments

We thank Lili Hamedi for her generous support. We are grateful to members of the Penzes lab for helpful discussions, especially Marc P. Forrest, Marc Dos Santos, Seyoun Yoon, and Euan Parnell for his help on the manuscript. Antonio Sanz-Clemente is gratefully acknowledged for providing access to his lab equipment. All experiments involving animals were performed according to the Institutional Animal Care and Use Committee of NU.

Conflict of interest

The authors declare that the research was conducted in the absence of any commercial or financial relationships that could be construed as a potential conflict of interest.

Publisher's note

All claims expressed in this article are solely those of the authors and do not necessarily represent those of their affiliated organizations, or those of the publisher, the editors and the reviewers. Any product that may be evaluated in this article, or claim that may be made by its manufacturer, is not guaranteed or endorsed by the publisher.

References

Bi, C., Wu, J., Jiang, T., Liu, Q., Cai, W., Yu, P., et al. (2012). Mutations of ANK3 identified by exome sequencing are associated with autism susceptibility. *Hum. Mutat.* 33, 1635–1638. doi: 10.1002/humu.22174

Cane, M., Maco, B., Knott, G., and Holtmaat, A. (2014). The relationship between PSD-95 clustering and spine stability in vivo. *J. Neurosci.* 34, 2075–2086. doi: 10.1523/JNEUROSCI.3353-13.2014

Crosby, K. C., Gookin, S. E., Garcia, J. D., Hahm, K. M., Dell'Acqua, M. L., and Smith, K. R. (2019). Nanoscale subsynaptic domains underlie the organization of the inhibitory synapse. *Cell Rep.* 26, 3284–3297.e3. doi: 10.1016/j.celrep.2019.02.070

Focking, M., Dicker, P., Lopez, L. M., Hryniewiecka, M., Wynne, K., English, J. A., et al. (2016). Proteomic analysis of the postsynaptic density implicates synaptic function and energy pathways in bipolar disorder. *Transl. Psychiatry* 6:e959. doi: 10.1038/tp.2016.224

Fujiwara, Y., Kondo, H. X., Shirota, M., Kobayashi, M., Takeshita, K., Nakagawa, A., et al. (2016). Structural basis for the membrane association of ankyrin G via palmitoylation. *Sci. Rep.* 6:23981. doi: 10.1038/srep23981

Gottschalk, M. G., Leussis, M. P., Ruland, T., Gjeluci, K., Petryshen, T. L., and Bahn, S. (2017). Lithium reverses behavioral and axonal transport-related changes associated with ANK3 bipolar disorder gene disruption. *Eur. Neuropsychopharmacol.* 27, 274–288. doi: 10.1016/j.euroneuro.2017.01.001

Grof, P., Duffy, A., Cavazzoni, P., Grof, E., Garnham, J., Mac Dougall, M., et al. (2002). Is response to prophylactic lithium a familial trait? *J. Clin. Psychiatry* 63, 942–947. doi: 10.4088/JCP.v63n1013

Hayashi, M. K., Tang, C., Verpelli, C., Narayanan, R., Stearns, M. H., Xu, R. M., et al. (2009). The postsynaptic density proteins Homer and Shank form a polymeric network structure. *Cells* 137, 159–171. doi: 10.1016/j.cell.2009.01.050

He, M., Abdi, K. M., and Bennett, V. (2014). Ankyrin-G palmitoylation and beta II-spectrin binding to phosphoinositide lipids drive lateral membrane assembly. *J. Cell Biol.* 206, 273–288. doi: 10.1083/jcb.201401016

He, M., Jenkins, P., and Bennett, V. (2012). Cysteine 70 of ankyrin-G is S-palmitoylated and is required for function of ankyrin-G in membrane domain assembly. *J. Biol. Chem.* 287, 43995–44005. doi: 10.1074/jbc.M112.417501

Hou, L., Heilbronner, U., Degenhardt, F., Adli, M., Akiyama, K., Akula, N., et al. (2016). Genetic variants associated with response to lithium treatment in bipolar disorder: a genome-wide association study. *Lancet* 387, 1085–1093. doi: 10.1016/S0140-6736(16)00143-4

Hughes, T., Sonderby, I. E., Polushina, T., Hansson, L., Holmgren, A., Athanasiu, L., et al. (2018). Elevated expression of a minor isoform of ANK3 is a risk factor for bipolar disorder. *Transl. Psychiatry* 8:210. doi: 10.1038/s41398-018-0175-x

Iqbal, Z., Vandeweyer, G., van der Voet, M., Waryah, A. M., Zahoor, M. Y., Besseling, J. A., et al. (2013). Homozygous and heterozygous disruptions of ANK3: at the crossroads of neurodevelopmental and psychiatric disorders. *Hum. Mol. Genet.* 22, 1960–1970. doi: 10.1093/hmg/ddt043

Jenkins, P. M., He, M., and Bennett, V. (2015a). Dynamic spectrin/ankyrin-G microdomains promote lateral membrane assembly by opposing endocytosis. *Sci. Adv.* 1:e1500301. doi: 10.1126/sciadv.1500301

Jenkins, P. M., Kim, N., Jones, S. L., Tseng, W. C., Svitkina, T. M., Yin, H. H., et al. (2015b). Giant ankyrin-G: a critical innovation in vertebrate evolution of fast and integrated neuronal signaling. *Proc. Natl. Acad. Sci. U. S. A.* 112, 957–964. doi: 10.1073/pnas.1416544112

Jenkins, P. M., Vasavda, C., Hostettler, J., Davis, J. Q., Abdi, K., and Bennett, V. (2013). E-cadherin polarity is determined by a multifunction motif mediating lateral membrane retention through ankyrin-G and apical-lateral transcytosis through clathrin. *J. Biol. Chem.* 288, 14018–14031. doi: 10.1074/jbc.M113.454439

Kang, R., Wan, J., Arstikaitis, P., Takahashi, H., Huang, K., Bailey, A. O., et al. (2008). Neural palmitoyl-proteomics reveals dynamic synaptic palmitoylation. *Nature* 456, 904–909. doi: 10.1038/nature07605

Kato, T., Hayashi-Takagi, A., Toyota, T., Yoshikawa, T., and Iwamoto, K. (2011). Gene expression analysis in lymphoblastoid cells as a potential biomarker of bipolar disorder. *J. Hum. Genet.* 56, 779–783. doi: 10.1038/jhg.2011.101

Khayachi, A., Ase, A., Liao, C., Kamesh, A., Kuhlmann, N., Schorova, L., et al. (2021). Chronic lithium treatment alters the excitatory/inhibitory balance of synaptic networks and reduces mGluR5-PKC signalling in mouse cortical neurons. *J. Psychiatry Neurosci.* 46, E402–E414. doi: 10.1503/jpn.200185

Kizhatil, K., Davis, J. Q., Davis, L., Hoffman, J., Hogan, B. L., and Bennett, V. (2007a). Ankyrin-G is a molecular partner of E-cadherin in epithelial cells and early embryos. *J. Biol. Chem.* 282, 26552–26561. doi: 10.1074/jbc.M703158200

Kizhatil, K., Yoon, W., Mohler, P. J., Davis, L. H., Hoffman, J. A., and Bennett, V. (2007b). Ankyrin-G and beta 2-spectrin collaborate in biogenesis of lateral membrane of human bronchial epithelial cells. *J. Biol. Chem.* 282, 2029–2037. doi: 10.1074/jbc.M608921200

Klein, P. S., and Melton, D. A. (1996). A molecular mechanism for the effect of lithium on development. *Proc. Natl. Acad. Sci. U. S. A.* 93, 8455–8459. doi: 10.1073/pnas.93.16.8455

Leterrier, C., and Dargent, B. (2014). No Pasaran! Role of the axon initial segment in the regulation of protein transport and the maintenance of axonal identity. *Semin. Cell Dev. Biol.* 27, 44–51. doi: 10.1016/j.semcdb.2013.11.001

Leussis, M. P., Berry-Scott, E. M., Saito, M., Jhuang, H., de Haan, G., Alkan, O., et al. (2013). The ANK3 bipolar disorder gene regulates psychiatric-related behaviors that are modulated by lithium and stress. *Biol. Psychiatry* 73, 683–690. doi: 10.1016/j.biopsych.2012.10.016

Lopez, A. Y., Wang, X., Xu, M., Maheshwari, A., Curry, D., Lam, S., et al. (2017). Ankyrin-G isoform imbalance and interneuronopathy link epilepsy and bipolar disorder. *Mol. Psychiatry* 22, 1464–1472. doi: 10.1038/mp.2016.233

Malhi, G. S., Gessler, D., and Outhred, T. (2017). The use of lithium for the treatment of bipolar disorder: recommendations from clinical practice guidelines. *J. Affect. Disord.* 217, 266–280. doi: 10.1016/j.jad.2017.03.052

Meyer, D., Bonhoeffer, T., and Scheuss, V. (2014). Balance and stability of synaptic structures during synaptic plasticity. *Neuron* 82, 430–443. doi: 10.1016/j.neuron.2014.02.031

Muhleisen, T. W., Leber, M., Schulze, T. G., Strohmaier, J., Degenhardt, F., Treutlein, J., et al. (2014). Genome-wide association study reveals two new risk loci for bipolar disorder. *Nat. Commun.* 5:3339. doi: 10.1038/ncomms4339

Nelson, A. D., and Jenkins, P. M. (2017). Axonal membranes and their domains: assembly and function of the axon initial segment and node of Ranvier. *Front. Cell. Neurosci.* 11:136. doi: 10.3389/fncel.2017.00136

Otani, K., Ujike, H., Tanaka, Y., Morita, Y., Kishimoto, M., Morio, A., et al. (2005). The ZDHHC8 gene did not associate with bipolar disorder or schizophrenia. *Neurosci. Lett.* 390, 166–170. doi: 10.1016/j.neulet.2005.08.019

Piguel, N. H., Yoon, S., Gao, R., Horan, K. E., Garza, J. C., Petryshen, T. L., et al. (2022). Lithium rescues dendritic abnormalities in Ank 3 deficiency models through the synergic effects of GSK3beta and cyclic AMP signaling pathways. *Neuropsychopharmacology*. doi: 10.1038/s41386-022-01502-2

Qin, X., Chen, J., and Zhou, T. (2020). 22q11.2 deletion syndrome and schizophrenia. *Acta Biochim. Biophys. Sin.* 52, 1181–1190. doi: 10.1093/abbs/gmaa113

Rao, A. S., Kremenevskaja, N., Resch, J., and Brabant, G. (2005). Lithium stimulates proliferation in cultured thyrocytes by activating Wnt/beta-catenin signalling. *Eur. J. Endocrinol.* 153, 929–938. doi: 10.1530/eje.1.02038

Roby, Y. (2017). ANK3 gene polymorphisms and bipolar disorder: a meta-analysis. *Psychiatr. Genet.* 27, 225–235. doi: 10.1097/YPG.0000000000000186

Rueckert, E. H., Barker, D., Ruderfer, D., Bergen, S. E., O'Dushlaine, C., Luce, C. J., et al. (2013). Cis-acting regulation of brain-specific ANK3 gene expression by a genetic variant associated with bipolar disorder. *Mol. Psychiatry* 18, 922–929. doi: 10.1038/mp.2012.104

Rusch, M., Zimmermann, T. J., Burger, M., Dekker, F. J., Gormer, K., Triola, G., et al. (2011). Identification of acyl protein thioesterases 1 and 2 as the cellular targets of the Ras-signaling modulators palmostatin B and M. *Angew. Chem. Int. Ed. Engl.* 50, 9838–9842. doi: 10.1002/anie.201102967

Salaun, C., Greaves, J., and Chamberlain, L. H. (2010). The intracellular dynamic of protein palmitoylation. *J. Cell Biol.* 191, 1229–1238. doi: 10.1083/jcb.201008160

Schulze, T. G., Detera-Wadleigh, S. D., Akula, N., Gupta, A., Kassem, L., Steele, J., et al. (2009). Two variants in Ankyrin 3 (ANK3) are independent genetic risk factors for bipolar disorder. *Mol. Psychiatry* 14, 487–491. doi: 10.1038/mp.2008.134

Scott, L. J., Muglia, P., Kong, X. Q., Guan, W., Flickinger, M., Upmanyu, R., et al. (2009). Genome-wide association and meta-analysis of bipolar disorder in individuals of European ancestry. *Proc. Natl. Acad. Sci. U. S. A.* 106, 7501–7506. doi: 10.1073/pnas.0813386106

Shah, B. S., Shimell, J. J., and Bamji, S. X. (2019). Regulation of dendrite morphology and excitatory synapse formation by zDHHC15. *J. Cell Sci.* 132. doi: 10.1242/jcs.230052

Smith, E. N., Bloss, C. S., Badner, J. A., Barrett, T., Belmonte, P. L., Berrettini, W., et al. (2009). Genome-wide association study of bipolar disorder in European American and African American individuals. *Mol. Psychiatry* 14, 755–763. doi: 10.1038/mp.2009.43

Smith, K. R., Kopeikina, K. J., Fawcett-Patel, J. M., Leaderbrand, K., Gao, R., Schurmann, B., et al. (2014). Psychiatric risk factor ANK3/ankyrin-G nanodomains regulate the structure and function of glutamatergic synapses. *Neuron* 84, 399–415. doi: 10.1016/j.neuron.2014.10.010

Tesli, M., Koefoed, P., Athanasiu, L., Mattingsdal, M., Gustafsson, O., Agartz, I., et al. (2011). Association analysis of ANK3 gene variants in nordic bipolar disorder and schizophrenia case-control samples. *Am. J. Med. Genet. B Neuropsychiatr. Genet.* 156B, 969–974. doi: 10.1002/ajmg.b.31244

Thomas, G. M., Hayashi, T., Chiu, S. L., Chen, C. M., and Huganir, R. L. (2012). Palmitoylation by DHHC5/8 targets GRIP1 to dendritic endosomes to regulate AMPA-R trafficking. *Neuron* 73, 482–496. doi: 10.1016/j.neuron.2011.11.021

Thomas, G. M., Hayashi, T., Huganir, R. L., and Linden, D. J. (2013). DHHC8-dependent PICK1 palmitoylation is required for induction of cerebellar long-term synaptic depression. *J. Neurosci.* 33, 15401–15407. doi: 10.1523/JNEUROSCI.1283-13.2013

Tortosa, E., and Hoogenraad, C. C. (2018). Polarized trafficking: the palmitoylation cycle distributes cytoplasmic proteins to distinct neuronal compartments. *Curr. Opin. Cell Biol.* 50, 64–71. doi: 10.1016/j.ceb.2018.02.004

Tseng, W. C., Jenkins, P. M., Tanaka, M., Mooney, R., and Bennett, V. (2015). Giant ankyrin-G stabilizes somatodendritic GABAergic synapses through opposing endocytosis of GABAA receptors. *Proc. Natl. Acad. Sci. U. S. A.* 112, 1214–1219. doi: 10.1073/pnas.1417989112

Wirgenes, K. V., Tesli, M., Inderhaug, E., Athanasiu, L., Agartz, I., Melle, I., et al. (2014). ANK3 gene expression in bipolar disorder and schizophrenia. *Br. J. Psychiatry* 205, 244–245. doi: 10.1192/bjp.bp.114.145433

Woods, G. F., Oh, W. C., Boudewyn, L. C., Mikula, S. K., and Zito, K. (2011). Loss of PSD-95 enrichment is not a prerequisite for spine retraction. *J. Neurosci.* 31, 12129–12138. doi: 10.1523/JNEUROSCI.6662-10.2011

Yang, Q., Zheng, F., Hu, Y., Yang, Y., Li, Y., Chen, G., et al. (2018). ZDHHC8 critically regulates seizure susceptibility in epilepsy. *Cell Death Dis.* 9:795. doi: 10.1038/s41419-018-0842-0

Yoon, S., Piguel, N. H., Khalatyan, N., Dionisio, L. E., Savas, J. N., and Penzes, P. (2021). Homer 1 promotes dendritic spine growth through ankyrin-G and its loss reshapes the synaptic proteome. *Mol. Psychiatry* 26, 1775–1789. doi: 10.1038/s41380-020-00991-1

Yuan, A., Yi, Z., Wang, Q., Sun, J., Li, Z., Du, Y., et al. (2012). ANK3 as a risk gene for schizophrenia: new data in Han Chinese and meta analysis. *Am. J. Med. Genet. B Neuropsychiatr. Genet.* 159B, 997–1005. doi: 10.1002/ajmg.b.32112

Zhang, X., and Bennett, V. (1998). Restriction of 480/270-kD ankyrin G to axon proximal segments requires multiple ankyrin G-specific domains. *J. Cell Biol.* 142, 1571–1581. doi: 10.1083/jcb.142.6.1571

Zhu, S., Cordner, Z. A., Xiong, J., Chiu, C. T., Artola, A., Zuo, Y., et al. (2017). Genetic disruption of ankyrin-G in adult mouse forebrain causes cortical synapse alteration and behavior reminiscent of bipolar disorder. *Proc. Natl. Acad. Sci. U. S. A.* 114, 10479–10484. doi: 10.1073/pnas.1700689114